Numerical study of dendritic growth during solidification using front-tracking method

Mohamad Ali JAAFAR[1,2], **Stéphane GIBOUT**[1], **Daniel ROUSSE**[2], **Jean-Pierre BÉDÉCARRATS**[1]
[1] Univ. Pau & Pays Adour – EA1932 – LATEP – Laboratoire de Thermique Energétique et Procédés, ENSGTI, Rue Jules Ferry, BP7511 – PAU, F-64075. France
[2] t3e Industrial Research Group, École de Technologie Supérieure, Montréal (Qc), Canada

E-mail: mohamadali.jaafar@univ-pau.fr, jaafar.mohamadali@gmail.com

Abstract. A two dimensional front-tracking method is developed in order to model dendritic growth during solidification processes of pure substances. The method uses a sequential set of moving marker points to describe and track the liquid-solid interface which evolves over a fixed background mesh describing the whole medium. The code behaviour is first checked by a simple stable case of solidification to provide homogeneous velocity at the interface. Then, test examples of unstable solidification cases considering different modes of anisotropy are performed. Finally, interface evolution, with primary and secondary branches, is described, showing the ability of the code to study realistic dendritic growth characteristics.

Keywords: Solidification process, Dendritic growth, Front-Tracking method.

1. Introduction

Solidification processes are involved in many industrial applications, mainly in metallurgy and thermal latent heat storage fields. In each application, solidified materials properties strongly depend on the dynamics of solidification. However, solidification can be either stable or unstable. Hence, in several circumstances, some materials may remain in their liquid states, even below the solid-liquid equilibrium temperature. The solidification, in this case, is thermodynamically unstable because supercooled liquid appears. Once the solid is nucleated through the supercooled liquid, after sufficient cooling for example, the solidification may involve a complex interplay of many physical effects. Many microstructures patterns may be produced depending mainly on the degree of supercooling; the difference between the equilibrium temperature and liquid temperature ($\Delta T = T_m - T_\infty$). When the supercooling degree is large enough, dendritic microstructure is commonly observed. That is due to the competition between the stabilizing effects at the solidification interface and the destabilizing effect of the supercooling. These stabilizing effects include mainly surface tension and kinetic mobility.
Understanding the mechanisms which result dendritic structures has been the objective of much research over the last decades. Many in-situ visualization studies were carried out for this purpose. R.R. Gilpin [1] has studied the dendritic growth in supercooled water in pipes. Water temperature at the nucleation instant was -3°C. He observed ice dendritic growth that evolved quickly from the nucleation center until the cross-section has been blocked. At the end of this phase the temperature of the remaining water in the pipe has returned to the equilibrium temperature i.e. 0°C. After that, no more dendritic ice growth has occurred, but an annulus of solid ice then began to grow slowly from the inside wall of the pipe toward the centre. Tirmizi and Gill [2] made some quantitative

measurements about ice crystals growth in pure water. The structures which were photographed changed sequentially from disks, to perturbed disks, to disk-dendrites, to partially developed dendrites, and finally to fully developed dendrites. Recently, Braga and Milon [3] have showed that dendritic growth appears only in supercooled liquid at the start of nucleation.

Numerically speaking, dendritic growth represents a pattern formation phenomenon, which in recent years has become a deeply researched subject in non-linear dynamics field. The principal difficulty while dealing with dendritic growth problem lies in the fact that the solidification interface constitutes both one of problem unknowns and one of the boundary conditions. Such problem is called a "moving boundary problem". Therefore, specific methods are required. These methods can be split according to the way in which they handle the moving boundary interface. The first class consists of keeping explicitly the data of the interfacial position using independent deforming grid that evolves with the solid-liquid interface. This front tracking method has been used by Juric and Tryggvason [4], for example. They developed a two dimensional method to model the dendritic solidification. The method was coupled with immersed boundary technique to distribute the heat sources at the interface over grid points nearest the interface during solidification. They produced some experimentally observed complex dendritic structures such as tip-splitting and side branching. Later, the method has been extended in order to include the convection effect [5].

From the other hand, some approaches have been also developed to model the dendritic growth. They track the interface by a supplementary parameter, usually varying from zero to unity. The main order parameter methods that are used for dendritic solidification problems are the level-set and phase-field methods. For the level-set method, the interface is represented by the zero value of the level-set function which is defined in the whole system. This method has been used by Chen et al. [6] and Gibou et al. [7], for example. The phase-field method, which has been used by Karma's team [8,9], for example, uses the phase-field variable which defines the physical state (liquid or solid) of a grid cell. The produced results showed that both of these methods are efficient to deal with the dendritic solidification problems.

Despite the large volume of literature dealing with dendritic growth and that the main basic principles are well understood, several questions remain without clear answers. For instance, what are the involved effects that make the dendrites choose their shapes?

In this context, the purpose of our work is to describe numerically, using front-tracking method, liquid-solid interface evolution, showing realistic phenomena, in terms of anisotropies and thermal liquid field effects during solidification process of pure substances. This paper focuses on the presentation of the solving procedure and its preliminary verification on reference cases. After a brief statement of the objectives and rationale behind the paper, the introduction provides a concise literature review. Then, sections 2 and 3 briefly present, respectively, the mathematical formulation of the problem and some numerical details. Section 4 discusses results while section 5 gives some concluding remarks.

2. Mathematical formulation

The present study deals with the idealized situation of dendritic solidification of pure substances, for which natural convection in the liquid is neglected. A horizontal two-dimensional mathematical model is considered in order to produce results that could be compared to the experimental results obtained with the experimental bench dedicated to this project[1]. The discontinuity of heat conductivity and heat capacity between solid and liquid phases is taken into account. The mass densities of liquid and solid phases are assumed to be equal and constant. Consequently, the mathematical model first involves the heat diffusion equation in both liquid and solid regions:

$$\rho c_s \frac{\partial(T)}{\partial t} = \vec{\nabla} \cdot \left(k_s \vec{\nabla} T\right) \qquad \text{solid region} \tag{1}$$

$$\rho c_l \frac{\partial(T)}{\partial t} = \vec{\nabla} \cdot \left(k_l \vec{\nabla} T\right) \qquad \text{liquid region} \tag{2}$$

[1] This device is still under construction, and is designed with small enough thickness along the ground-gravity axis to prevent movement in the third dimension.

where ρ is both liquid and solid density, c is the specific heat, and k is the thermal conductivity. s and l refer to the solid and liquid phases, respectively.
Second, the model involves the energy balance equation at the solid-liquid interface:

$$\rho L(T_f) v_n = \left(k_s \vec{\nabla} T_s - k_l \vec{\nabla} T_l\right) \cdot \vec{n} \tag{3}$$

where v_n is the normal velocity of the interface, $L(T_f)$ determines the latent heat in terms of the interface temperature (T_f) and is calculated by the following expression:

$$L(T_f) = L + (c_l - c_s)(T_f - T_m) \tag{4}$$

Finally, the model is completed with the temperature at the interface which can be evaluated by the following Gibbs-Thomson condition:

$$T_f = T_m - T_m \frac{\gamma(\theta)\kappa}{\rho L} - \frac{v_n}{\upsilon(\theta)} - T_m \frac{(c_l - c_s)}{L}\left(T_f \, ln\left(\frac{T_f}{T_m}\right) + Tm - T_f\right) \tag{5}$$

where κ is twice of interface mean local curvature, $\gamma(\theta)$ is the anisotropic surface tension, and $\upsilon(\theta)$ represents the anisotropic kinetic mobility. θ is the angle between the normal vector at the interface and an arbitrary reference axis.
The Gibbs-Thomson condition (eq. (5)) expresses the local thermodynamics equilibrium condition of the moving interface, taking into account the curvature as well as the anisotropies effects of surface tension and kinetic mobility.

3. Numerical method

The front-tracking method is chosen for this study. The main idea behind this method is that it resolves separately the energy equation in both liquid and solid phases, and the interface problem. Thus, it permits dividing the whole domain in three sub-domains: the liquid region, the solid region, and the moving interface in between. Secondly, this method uses lower dimension completely independent mesh to track the interface. Generally, this mesh is thinner than the global one used for the whole domain (solid and liquid regions). Therefore, the interface location can be tracked with precision independently of the global mesh. Finally, parallelization is possible with this method.
A finite volume method is implemented to discretize the heat partial differential equations in both liquid and solid phases, Eqs. (1) and (2). Herein, a square regular mesh is used for dividing solid and liquid regions in elementary volumes of unit thickness. Moreover, an explicit first-order forward Euler time integration method is used. Then, for each time step, temperature fields of solid and liquid cells are updated in terms of conductive heat flows from the other surrounding cells, as well as the latent heat released by the interface due to the solidification process.
The interface is represented by a moving set of marker points connected in a sequential order. Eqs (3) and (5) are then solved at each point of the moving mesh in order to evaluate its temperature and normal velocity. The temperature, on the one hand, is used to calculate the interface latent heat flow evacuated through the liquid and solid regions. On the other hand, the normal velocity is used to calculate the elementary displacement of each interface marker point. As the interface deforms greatly, the addition and suppression of marker points are required to maintain a good resolution for interface shape; a minimum and maximum distances between two adjacent points must then be defined. The maximum limit distance is generally calculated in terms of regular fixed grid cells dimensions so that one grid cell can contain several marker points.
Each grid cell is represented mainly by its volume, centroid, and side (i.e. exchange) surfaces. At each time step, information must be passed between the moving representation of the interface and the stationary grid of the whole domain. That is done by a geometrical step which calculate the geometrical properties of all the grid cells (liquid and solid phases), taking into account the position of the interface. For this purpose, the numerical algorithm must be able to distinguish between a grid cell in which the interface takes place and another in which the interface does not. Figure 1 presents, for instance, four adjacent grid cells. One of these grid cells (on the right bottom) does not contain an interface, and the three others do.

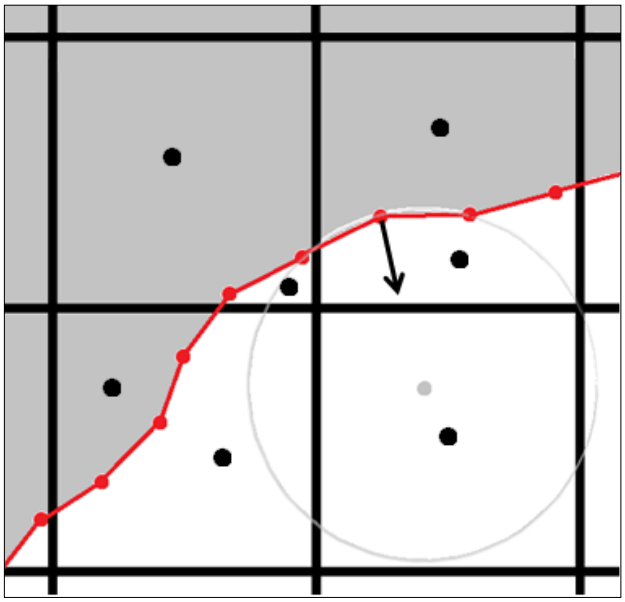

Figure 1. Four adjacent grid cells: (right bottom) without interface; (three others) with interface. The unique circle connecting three consecutive interface marker points to evaluate the curvature and the normal vector direction.

When dealing with a single-phase grid cell, through which interface does not pass (figure 1 – right bottom), all the geometrical properties can be deduced directly from the global thermal grid dimensions. On the other hand, the geometrical properties of grid cell into which an interface takes place (figure 1 – right top, left top, and left bottom), have to be properly evaluated. Both liquid (white) and solid (grey) coexist in such irregular grid cells. However, for each phase, all parameters which are needed for evaluating the temperature evolution are calculated. These parameters are volume, exchange side surfaces, interface length, and centroid location (black dots).
Then, local curvature and normal vector direction are obtained by constructing the unique circle which connects a marker point with its two neighbours (see example in figure 1). By convention, the normal vector is always considered to be oriented towards the liquid phase. Finally, surface tension and the inverse of kinetic mobility anisotropies are respectively given by [4]:

$$\gamma(\theta) = \gamma\left\{1 + A_\gamma\left[\frac{8}{3}sin^4\left(\frac{1}{2}m_\gamma(\theta - \theta_\gamma)\right) - 1\right]\right\} \tag{6}$$

$$\frac{1}{\upsilon(\theta)} = \left(\frac{1}{\upsilon}\right)\left\{1 + A_\upsilon\left[\frac{8}{3}sin^4\left(\frac{1}{2}m_\upsilon(\theta - \theta_\upsilon)\right) - 1\right]\right\} \tag{7}$$

where γ is the isotropic surface tension, υ is the isotropic kinetic mobility, A_γ and A_υ determine the magnitude of anisotropy of the surface tension and the kinetic mobility, respectively. m_γ and m_υ determine the mode of symmetry of the crystal. θ_γ and θ_υ determine the angle of symmetry axis with respect to a reference axis (horizontal axis is chosen).
From an initial given interface shape and temperature fields of liquid and solid phases, the numerical algorithm proceeds iteratively through the following main steps:

1. Updating the interface discretization: adding and deleting marker points.
2. Updating geometrical properties of the global grid cells: volume, centroid location, side surfaces, and length of the interface passing through.
3. Calculation of interface marker points characteristics: surface tension, kinetic mobility, curvature, normal vector, local temperature gradients.
4. Resolution of the interface problem, eqs (3-5): temperature and normal velocities.
5. Updating the temperature fields of the liquid and solid phases (eqs (2) and (1), respectively).
6. Moving the interface marker points.

The time step is considered constant over the whole iterative procedure. It is initially calculated in terms of both interface average velocity and regular grid cells dimensions. The time step must be selected so that several time steps are needed for an interface marker point to pass through a grid cell, and such that the convergence is ensured. The numerical algorithm is written in C++ using an object-oriented approach in order to simplify its future evolutions.

4. Results

This section presents and discusses selected results to avoid making the paper overly lengthy. These results are obtained by the numerical method described in the previous section in two space dimensions. The evolution of the liquid-solid interface during the solidification process of a supercooled pure substance is described. The solidification is initiated by introducing a small solid seed of radius R in the domain. Initially, solid temperature is assumed to be equal to the equilibrium fusion temperature T_m, and the domain contains a supercooled liquid at a homogeneous temperature $T_\infty < T_m$. For each problem, the physical parameters are presented, numerical details follow, and the result is then described and discussed.

4.1. *Stable solidification*

The numerical method must be able, first, to produce the circular symmetry test of the stable case of solidification, for which anisotropies effects are neglected. In such case, evolution of the interface is homogeneous and the developing structure retains its initial shape. Therefore, in order to check the code behaviour, a stable solidification case is studied. An initial solid circular seed ($R = 1\ \mu m$) is introduced at the centre of the supercooling liquid ($T_\infty = T_m - 10$). To neglect boundary conditions effects on the interface evolution, the boundaries are assumed to be adiabatic. The following figure represents results of interface evolution in this case. For computation time purposes, a small domain of 144 µm² is considered.

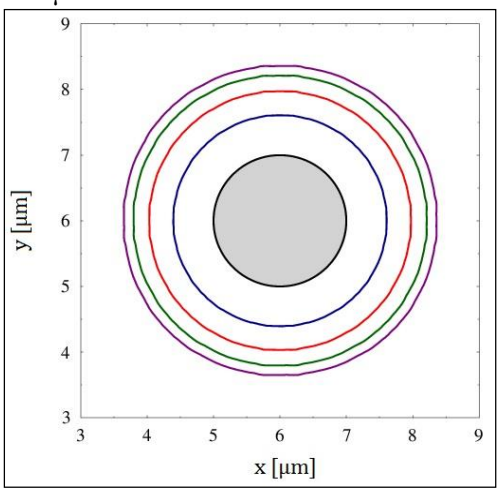

Figure 2. Evolution of the interface for stable solidification. Time interval between lines is 0.05 ms.

In figure 2, with isotropic surface tension and kinetic mobility, the interface develops homogeneously retaining its initial shape. Indeed, at each time step, marker points have the same radius forming a circle for which radius increases with time. In this case, the growing interface temperature also maintains the equilibrium temperature. Thus, there is no heat transfer between the interface and the solid phase. These thermal conditions are similar to those of Stefan solidification problem. Consequently, the shape obtained here validates the numerical code, producing, for a stable case, homogeneous velocities of all interface marker points.

4.2. *Unstable solidification: symmetry and primary branches*

Unstable solidification may be produced assuming anisotropic surface tension and kinetic mobility, given by eqs. (6) and (7), respectively. In order to check the code behaviour and the numerical method implementation in this case, two different modes of anisotropy are considered. Under the same

geometrical and thermal conditions, figures 3 and 4 represent unstable liquid-solid interface evolution with four-fold ($m_\gamma = m_\upsilon = 4$) and six-fold ($m_\gamma = m_\upsilon = 6$) anisotropies, respectively. An initial solid seed ($R = 1\ \mu m$) is introduced at the centre of the supercooled liquid ($\Delta T = 10\ K$). To ensure a continuous evolution of the interface, a slightly smaller temperature is imposed on the domain boundaries ($T_\infty - 2K$). A domain of 2500 µm² is considered for both computations.

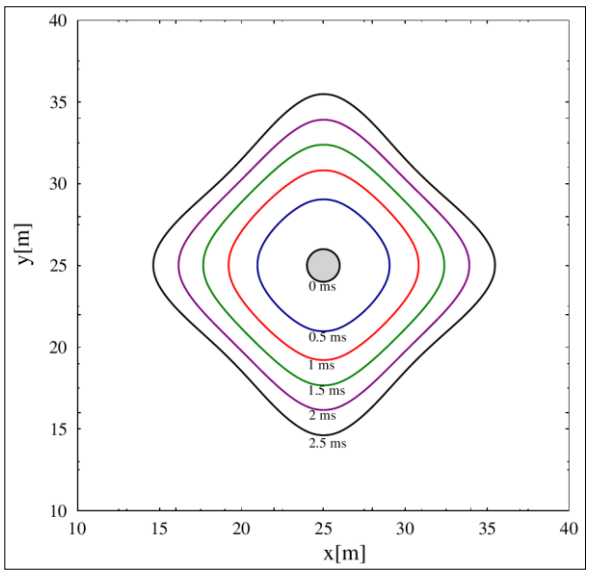

Figure 3. Evolution of the interface with four-fold anisotropy. $m_\gamma = m_\upsilon = 4$. $\theta_\gamma = \theta_\upsilon = 0$. Time interval is 0.5 ms.

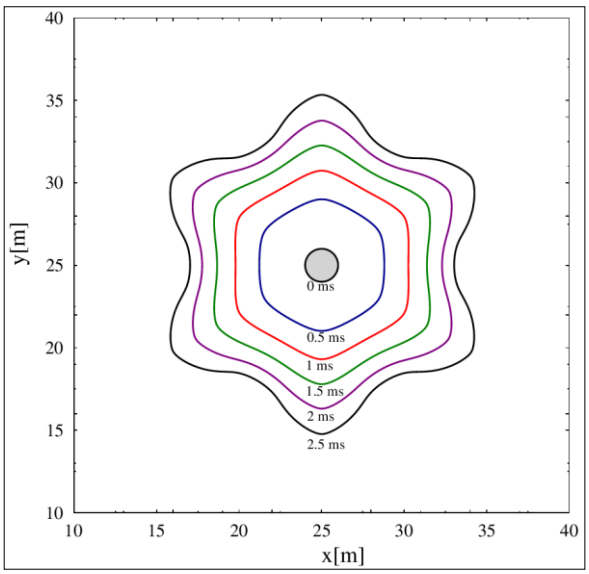

Figure 4. Evolution of the interface with six-fold anisotropy. $m_\gamma = m_\upsilon = 6$. $\theta_\gamma = \theta_\upsilon = \frac{\pi}{6}$. Time interval is 0.5 ms.

In contrast to figure 2, these results represent non-homogeneous interface evolution. The growing interface does not have the memory of its initial shape, and, depending on the anisotropy mode, privileged growth directions appear. In figure 3, in which four-fold anisotropy is considered, the interface has grown in four particular directions according to x-axis (reference axis) depending on anisotropies expressions parameters. However, in figure 4, which considers ice-flake anisotropy mode (six-fold), six privileged growth directions have appeared. Both results show interface deformations from first stages of computation according to anisotropies modes. These primary branches and particular growth directions demonstrate the correctness of the numerical method implementation and that the code appropriately reacts when dealing with unstable cases of solidification. The results showing primary branches symmetry partially validate the ability of the numerical code to deal with dendritic growth. However, it is essential to test the interface behaviour in somewhat more advanced stages to provide secondary branches. Secondary branches or larger order of branches are due to the interaction between thermal and anisotropies effects. Consequently, producing these branches shows that the numerical code is able to produce the first stages of realistic dendritic growth.

4.3. *Unstable solidification: secondary branches*

Due to symmetry and time computation purposes, in this problem, the computational domain is restricted to the positive quadrant. Further, a symmetry axis is imposed along the diagonal-axis of the domain to benefit from maximum possible space that could be given to the growing interface. Figure 5 thus presents an advanced interface evolution growing from same solid seed radius (1 µm), but in supercooled liquid with $\Delta T = 8\ K$. Slightly smaller temperature is imposed on the right and top domain boundaries ($T_\infty - 1K$), and adiabatic conditions are assumed elsewhere. A domain of 2500 µm² is considered. Figures 6, 7, and 8 represent the liquid phase temperature fields at different stages of computation.

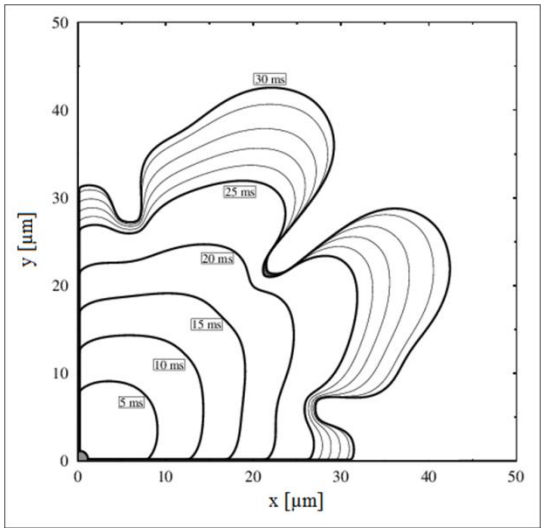

Figure 5. Evolution of the interface in the positive quadrant with four-fold anisotropy. $m_\gamma = m_\upsilon = 4$. $\theta_\gamma = \theta_\upsilon = \frac{\pi}{4}$. Time interval of bold interfaces is 5 ms.

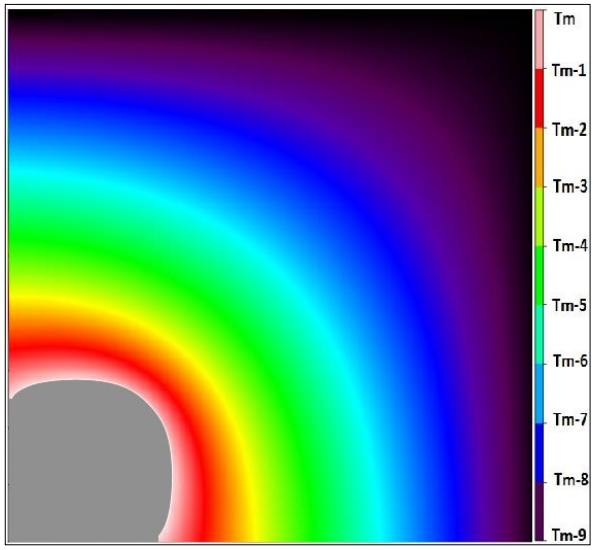

Figure 6. Temperature field in liquid phase at 10 ms.

In figure 5, realistic dendritic growth behaviour can be clearly observed. From early computation stages (5, 10, and 15 ms), a large branch appears along the diagonal-axis depending on anisotropies surface tension and kinetic mobility expressions parameters ($m_\gamma = m_\upsilon = 4 \; and \; \theta_\gamma = \theta_\upsilon = \frac{\pi}{4}$). In figure 6, the liquid thermal field shows that, at 10 ms the local thermal gradient at the interface in the normal vector direction is homogeneous. Therefore, one can deduce that thermal gradient has no effect on the interface evolution at these early stages, but only anisotropies effects govern the evolution of the interface to choose the diagonal-axis as privileged growth direction. Further, at 20 ms, three deformations appear, at the tip and on both sides of the interface. At this stage, in figure 7, the homogeneous thermal gradient with liquid phase near the interface begins to break, providing tip-splitting and secondary branches at the interface sides. At 25 ms, figure 8 presents an increase in the liquid temperature in the vicinity of the cavities at the branch-tip and interface sides (shown in pale pink). Increase in temperature prevents thereafter interface growing toward regions involving this temperature, providing then realistic dendritic shapes at stages between 25 and 30 ms (figure 5). These realistic phenomena (tip-splitting and secondary branches) show the appropriate interaction between stabilizing and destabilizing effects at the interface for unstable case of solidification. They therefore validate the ability of the numerical code to provide realistic dendritic growth and to study its characteristics.

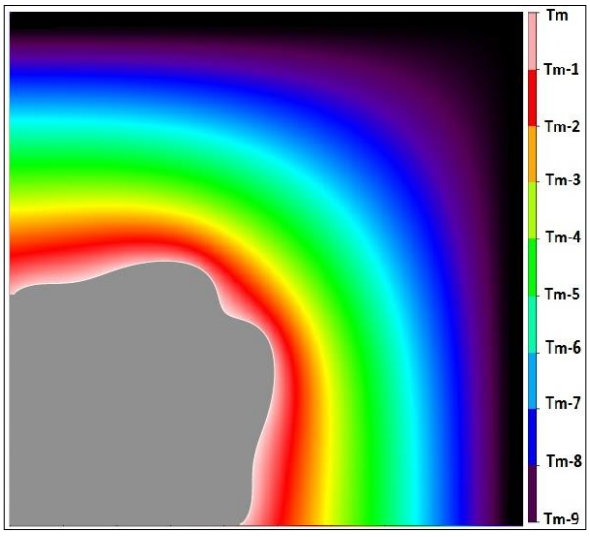

Figure 7. Temperature field in liquid phase at 20 ms.

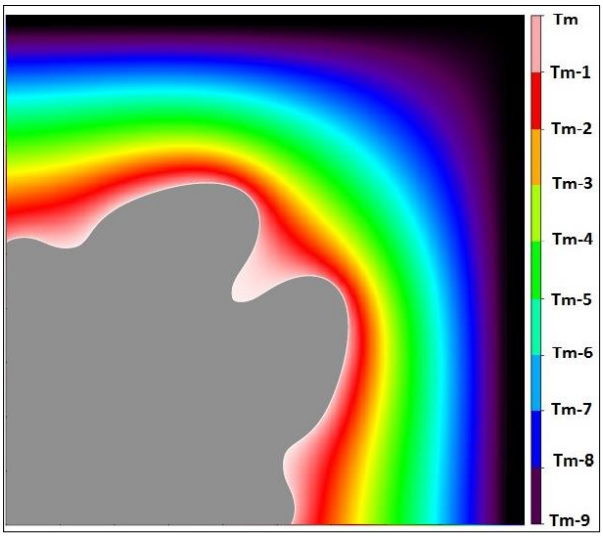

Figure 8. Temperature field in liquid phase at 25 ms.

5. Conclusions

This paper deals with the solidification process of pure substances that is involved in several industrial applications. The interaction between thermal and anisotropies effects, which provides dendritic growth pattern, is described numerically in order to investigate what affects the dendrite growth directions, and what is the influence of the thermal behaviour on this growth. The study limits its scope to growth in a two-dimensional environment, free from natural convection.

The mathematical model is based upon the heat diffusion equations in both phases, a heat balance at the solid-liquid interface, and the Gibbs-Thomson condition. The numerical method is based on the explicit front-tracking approach. It is embedded in a finite volume formulation in which an explicit first-order forward Euler time integration is used. The moving interface is represented by a moving set of maker points connected in a sequential order.

The numerical code is first checked, by use a simple stable case of solidification, for which homogeneous velocities at the interface are produced. Then, two different anisotropies modes are performed in order to test the code behaviour to provide appropriate privileged directions and primary branches. Finally, an advanced unstable case of solidification is performed, for which the interface evolution is described. Results show that the code is able to deal with some particular cases of dendritic growth, providing realistic phenomena as tip-splitting and secondary branches.

Upcoming works involve, in the one hand, quantitative validation of the numerical code, as well as, more advanced numerical results considering some particular cases of dendritic growth, and on the other hand, the design of a two-dimensional test bench in attempt to compare experimental visualisation to numerical results obtained with the proposed method.

References

[1] Gilpin R R 1977 The effects of dendritic ice formation in water pipes *International Journal of Heat and Mass Transfer* **20** 693
[2] Tirmizi S H and Gill W N 1978 Effect of natural convection on growth velocity and morphology of dendritic ice crystals *Journal of Crystal Growth* **85** 488
[3] Braga S L and Milon J J 2012 Visualization of dendritic ice growth in supercooled water inside cylindrical capsules *International Journal of Heat and Mass Transfer* **55** 3694
[4] Juric D and Tryggvason G 1996 A front-tracking method for dendritic solidification *Journal of Computational physics* **123** 127
[5] Al-Rawahi N and Tryggvason G 2004 Numerical simulation of dendritic solidification with convection: Three-dimensional flow *Journal of Computational physics* **194** 677
[6] Chen S Merriman B Osher S and Smereka P 1997 A simple level set method for solving Stefan problems *Journal of Computational physics* **135** 8
[7] Gibou F Fedkiw R Caflisch R and Osher S 2003 A level set approach for the numerical simulation of dendritic growth *Journal of Scientific Computing* **19** 183
[8] Karma A and Rappel W J 1996 Phase-field method for computationally efficient modeling of solidification with arbitrary interface kinetics *Physical Review E* **53** 3017
[9] Karma A and Rappel W J 1998 Quantative phase-field modeling of dendritic growth in two and three dimensions *Physical Review E* **57** 4323